

Support Information

Single-Atom Molybdenum Doping Induces Nickel Oxide-to-Hydroxide Transformation for Enhanced Alkaline Hydrogen Evolution

Yuanqi Liu,^a Qiang Gao,^b Lei Shi,^b Joseph Kearney,^b Xue Han,^c Zhenhua Xie,^d Maoyu Wang,^e Hua
Zhou,^e and Huiyuan Zhu^{*ab}

^a *Department of Chemical Engineering, University of Virginia, Charlottesville, VA 22903, USA.*

^b *Department of Chemistry, University of Virginia, Charlottesville, VA 22904, USA.*

^c *Chemistry Division, Brookhaven National Laboratory, Upton, New York 11973, USA.*

^d *Department of Chemical Engineering, Columbia University, New York, New York 10027, USA.*

^e *X-ray Science Division, Advanced Photon Source, Argonne National Laboratory, Lemont, IL 60439,
USA.*

Experimental Section

Materials

Nickel (II) acetylacetonate ($\text{Ni}(\text{acac})_2$, 95%), molybdenum hexacarbonyl ($\text{Mo}(\text{CO})_6$, 98%), oleylamine (OAm, 70%), potassium hydroxide (KOH, 90%) were all purchased from Sigma–Aldrich. Hexane and ethanol were technical grade and used as received without further purification. Nafion D520CS solution (5 wt%) were purchased from Ion Power. Carbon black–Vulcan XC 72R, carbon paper - Toray Carbon Paper 060 with micro porous layer, and commercial Pt - 20% platinum on carbon XC-72 were purchased from Fuel Cell Store.

Synthesis of Mo-NiO Nanoparticles (NPs), MoO_3/NiO NPs and Catalyst Preparation

In a typical procedure, 0.4 mmol $\text{Ni}(\text{acac})_2$, 0.1 mmol $\text{Mo}(\text{CO})_6$ precursor and 15 ml OAm were added into a 50 ml three-necked flask under stirring. The mixture was heated under N_2 atmosphere to 100 °C and kept at this temperature for 15 min. Then the solution was further heated to 280 °C at a ramping rate of 10 °C/min and incubated at this temperature for 1 h, generating a reddish solution. After cooling down to room temperature, the precipitate was centrifuged and washed two times with hexane and excess ethanol and then dispersed in hexane. To prepare carbon-supported catalysts, we mixed a hexane dispersion of 10 mg NPs with 40 mg carbon black (Vulcan XC 72R) and sonicated for 2 h. The catalysts were collected by centrifugation and dried for 12 h in a vacuum oven at room temperature. Finally, the carbon-supported catalyst was annealed in air at 350°C for 12 h to remove the surfactants and then collected in a powder form.

For the MoO_3/NiO NPs, the synthesis procedure was identical to that of Mo-NiO NPs, with the exception that the precursor amounts were 0.1 mmol of $\text{Ni}(\text{acac})_2$, 0.4 mmol of $\text{Mo}(\text{CO})_6$. For the 2% Mo doped Mo-NiO NPs, the synthesis procedure was identical to that of Mo-NiO NPs, with the exception that the precursor amounts were 0.4 mmol of $\text{Ni}(\text{acac})_2$, 0.05 mmol of $\text{Mo}(\text{CO})_6$. For the 9% Mo doped Mo-NiO NPs, the synthesis procedure was identical to that of Mo-NiO NPs, with the exception that the precursor amounts were 0.4 mmol of $\text{Ni}(\text{acac})_2$, 0.2 mmol of $\text{Mo}(\text{CO})_6$. For the NiO NPs, the synthesis procedure was identical to that of Mo-NiO NPs, with the exception that no $\text{Mo}(\text{CO})_6$ precursor was added.

For the catalyst ink preparation, 25 mg of carbon-supported catalyst was dispersed in 1 ml isopropanol with 0.1 ml of Nafion solution, and the mixture was then ultrasonicated for at least 30 min to generate a homogeneous ink. Subsequently, 0.2 ml of the dispersion was transferred onto 1 cm^2 carbon paper, leading to a metal loading of $\sim 1 \text{ mg}/\text{cm}^2$.

Characterization

X-ray Diffraction patterns (XRD) were obtained from Empyrean X-Ray Diffractometer which used a Cu anode (1.54 Å wavelength) and operated at 45 kV and 40 mA. The crystallite size of Mo-NiO NPs

and NiO NPs are determined by Debye Scherrer's equation ($D = \frac{K\lambda}{\beta \cos\theta}$), where D is the crystallite

size, K is the Scherrer constant (0.9), λ is the wavelength of the X-ray used (Cu $K\alpha$ 1.54056 Å), β is the Full Width at Half Maximum (FWHM) and θ is the Bragg angle. Transmission electron microscopy (TEM) images were obtained from FEI Tecnai Spirit (120 kV & 2k × 2k UltraScan CCD camera). High-angle annular dark-field scanning TEM (HAADF-STEM) results were obtained from Thermo Fisher Scientific Themis Z. The element contents of samples were obtained from inductively coupled plasma optical emission spectrometry on a Avio 200 Scott ICP-OES. The X-ray absorption spectra (XAS) of Ni and Mo K-edges were obtained at beamline 7-BM (QAS) of the National Synchrotron Light Sources II (NSLS-II) at Brookhaven National Laboratory. The XAS of NiO samples were obtained at beamline 12-BM-B of the Advanced Photon Source (APS) at Argonne National Laboratory. All XAS data analyses were performed with the Athena and Artemis software package to extract X-ray Absorption Near Edge Structure (XANES) and Extended X-ray Absorption Fine Structure (EXAFS). X-ray photoelectron spectrum (XPS) was performed on a PHI Versa Probe III scanning XPS microscope using a monochromatic Al K-alpha X-ray source (1486.6 eV).

***In situ* XAS experiments**

The Ni and Mo K-edge spectra were obtained in fluorescence mode using a passivated implanted planar silicon (PIPS) detector. Typically, the Mo-NiO NPs ink was coated on carbon paper (1 × 1 cm²) with the metal loading of 0.5 mg/cm² as the working electrode. The data were recorded under different applied potentials of open circuit potential (OCP), -0.1, -0.2, and -0.4 V vs RHE. The duration for a single spectrum was around 1 min, and 15 spectra were merged to improve the signal-to-noise ratio. Ni and Mo foils, as the standard references, were employed to calibrate energy shifts and obtain the passive electron reduction factor (S_0^2) used for the EXAFS fitting.

***In situ* Raman spectrometry measurements**

In-situ Raman measurements were carried out jointly by an inVia-Reflex (Renishaw, 785 nm) and a Metrohm electrochemical workstation NOVA2. A home-made three-electrode electrochemical cell was used as the reactor for the *in situ* measurements. The obtained electrodes (1 × 1 cm² coated with sample ink), Hg/HgO electrode, and graphite rod served as the working electrode, reference electrode, and counter electrode, respectively. The working electrode was immersed into the electrolyte and the electrode plane was maintained perpendicular to the laser. *In-situ* Raman spectra were collected without potential applied (*ex-situ*) and under different applied potentials of OCP, -0.1V, -0.2V and -0.4V vs. RHE.

Electrochemical measurements

Electrochemical measurements were performed using a three-electrode system connected to a BioLogic electrochemical workstation. All measurements were performed at room temperature under Ar atmosphere. The electrolyte was 1 M KOH, and the working electrode was the (1 x 1 cm² carbon paper) carbon paper loaded with loading catalysts. The graphite rod and Hg/HgO (1M KOH) were used as the counter and reference electrode, respectively. All the potentials in this study were referenced to the RHE. The Hg/HgO electrode potential was converted to RHE according to E (versus RHE) = E (versus Hg/HgO) + 0.198 V + 0.059 × pH. Linear scan voltammetry curves (LSV) were

obtained at a scan rate of 5 mV/s. In this work, 85% iR correction was conducted for all LSV curves. The linear part of the Tafel plot was simulated polarization curve by the Tafel equation ($\eta = b \log[i] + a$) to obtain the Tafel slope. The CV curves at different scan rates (20 mV/s - 100 mV/s) were linearly fitted to obtain C_{dl} , and the electrochemically active surface area (ECSA) was obtained by further calculations ($ECSA = C_{dl}/C_s$, $C_s = 0.04 \text{ mF/cm}^2$). The electrochemical impedance spectroscopy (EIS) was performed in the same configuration at - 0.2 V vs. RHE applied potential over frequency range from 100 kHz to 0.1 Hz at the amplitude of the sinusoidal voltage of 5 mV. The stability test was measured by the chronoamperometry. The cycling durability of the Mo-NiO NPs was evaluated by potential cycling between 0 and -0.3 V for 3000 cycles at a scan rate of 50 mV/s.

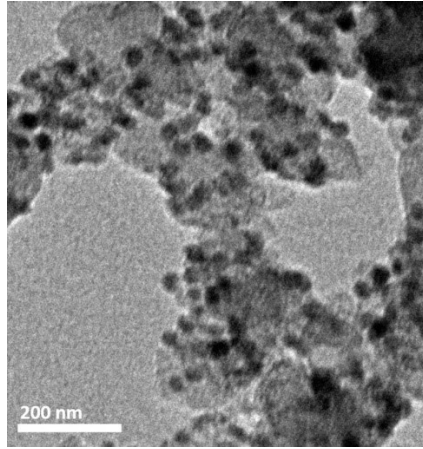


Figure S1. The BF-TEM image of Mo-NiO NPs loading on Vulcan XC 72R after air annealing.

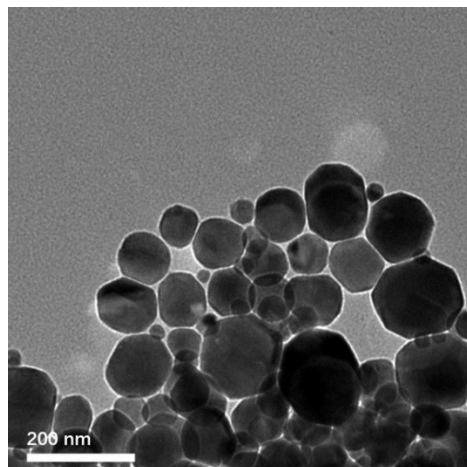


Figure S2. The BF-TEM image of NiO NPs.

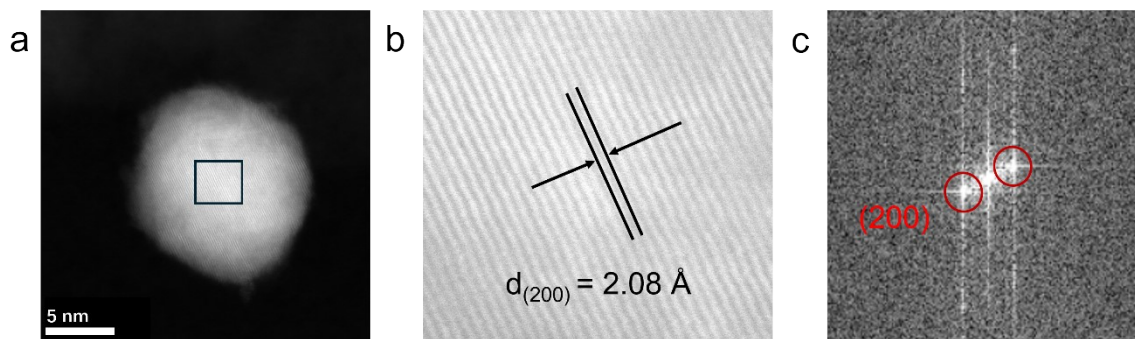


Figure S3. a-b) HR-TEM, c) FFT pattern of Mo-NiO NPs.

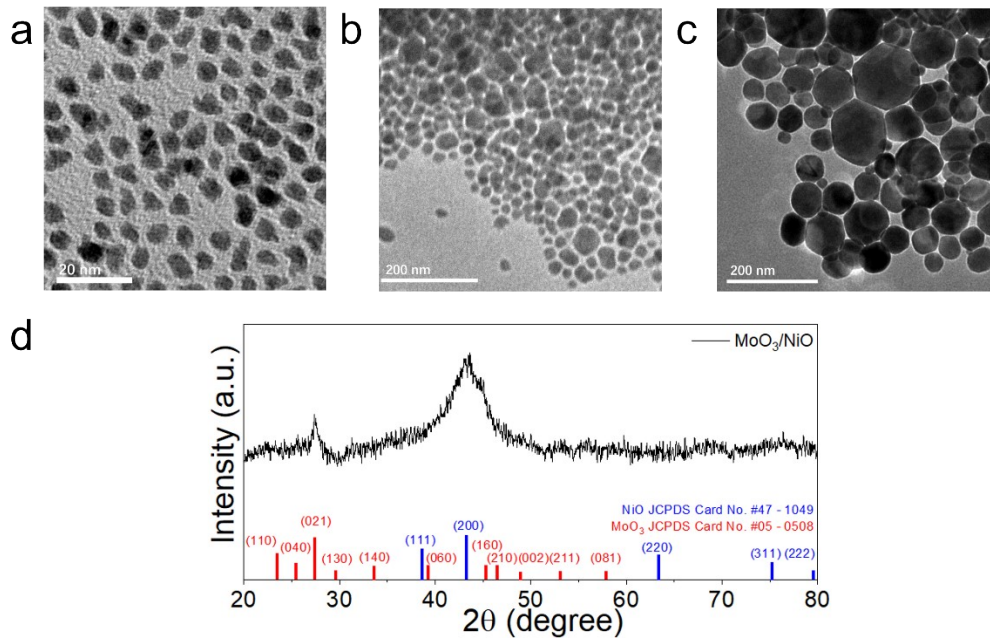


Figure S4. a-c) The BF-TEM image of MoO₃/NiO NPs, 9% Mo-NiO NPs and 2% Mo-NiO NPs. d) XRD pattern of MoO₃/NiO.

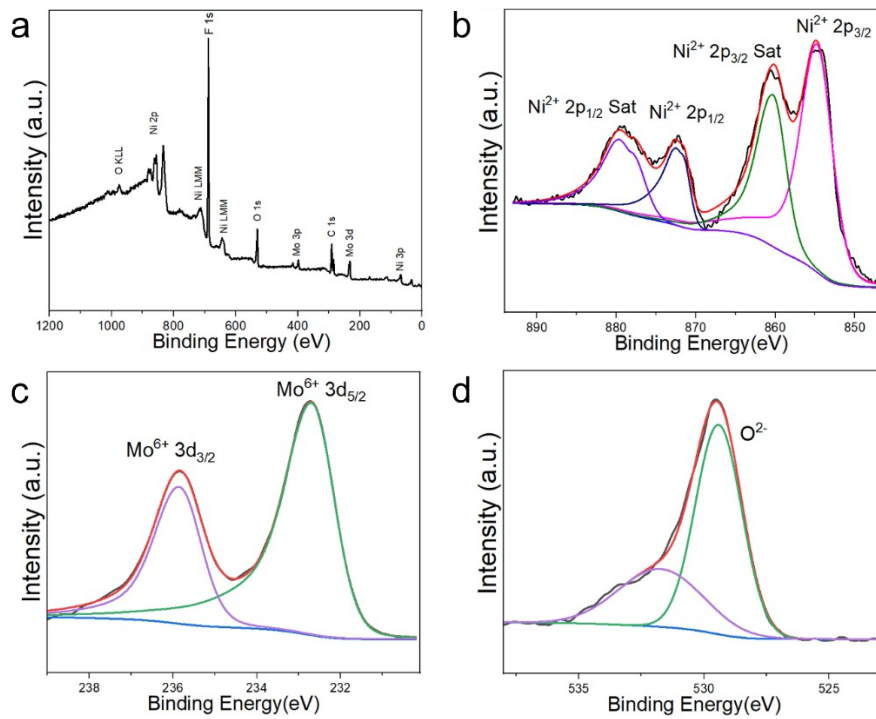


Figure S5. a) XPS survey spectra, b) Ni 2p XPS spectra, c) Mo 3d spectra, d) O 1s spectra of Mo-NiO NPs.

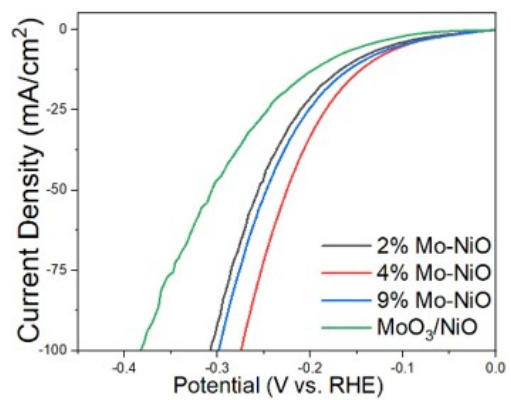


Figure S6. LSV curves of MoO₃/NiO NPs, 9% Mo-NiO NPs and 2% Mo-NiO NPs. .

Table S1. Comparison of HER activity with previous reports.

Catalysts	Overpotential @ 10mA/cm ²	Tafel slope	Reference
Mo-NiO	131 mV	117 mV/dec	this work
NiON	129 mV	34 mV/dec	1
N ₁₃₀ -Ni(OH) ₂ /NF	239 mV	109 mV/dec	2
Ni/Fe-MoS ₂ /CC	116 mV	43 mV/dec	3
NiMoO ₄ @g-CN-600	148 mV	97 mV/dec	4
Ni-MoS ₂	160 mV	79 mV/dec	5
Ni(OH) ₂ @Fe _x Co _{1-x} Pi NiO	171 mV	N/A	6
NiMoO ₄ /MoO ₂	162 mV	123 mV/dec	7
BSCMo _{0.1} O _{3-δ}	243 mV	101.2 mV/dec	8
SCG(200)@NiMo	127 mV	117 mV/dec	9

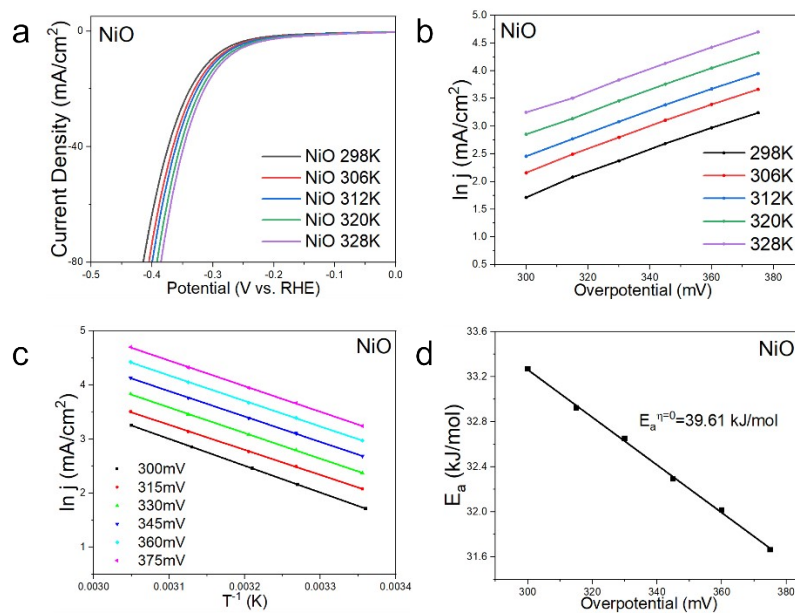


Figure S7. a) LSV curves obtained at different temperature, b) The $\ln j$ vs. η plots obtained at different temperature, c) The corresponding Arrhenius plots at different η , d) The variation of E_a as a function of η on NiO NPs.

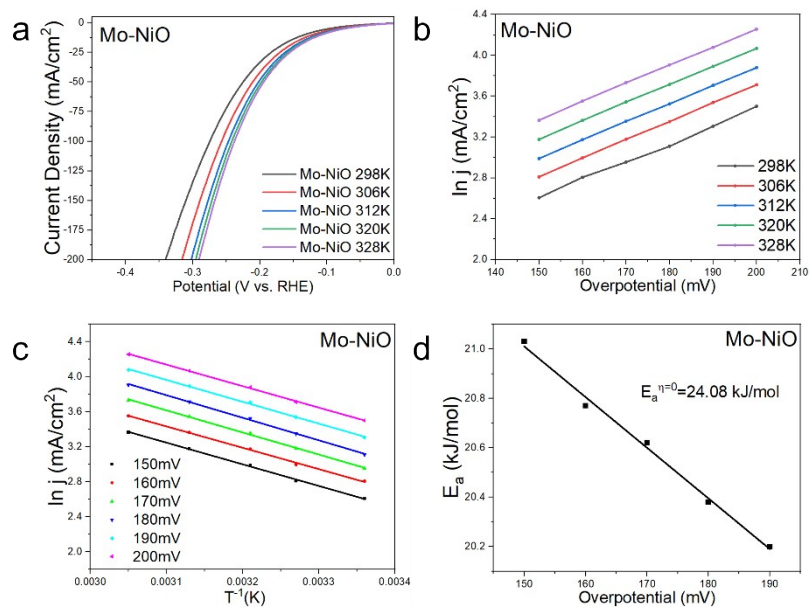


Figure S8. a) LSV curves obtained at different temperature, b) The $\ln j$ vs. η plots obtained at different temperature, c) The corresponding Arrhenius plots at different η , d) The variation of E_a as a function of η on Mo-NiO NPs.

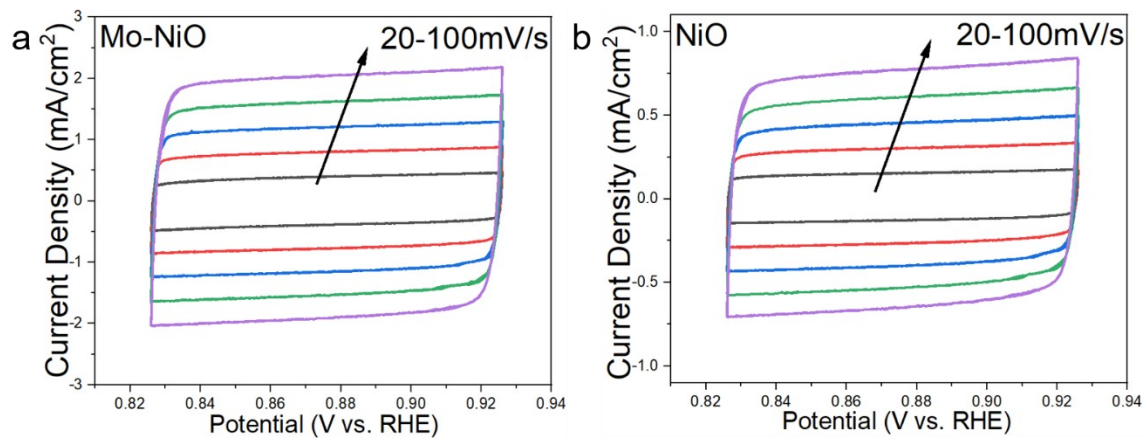


Figure S9. Capacitance measurement. Cyclic voltammograms in the region of 0.826-0.926 V vs. RHE for a) Mo-NiO NPs, b) NiO NPs.

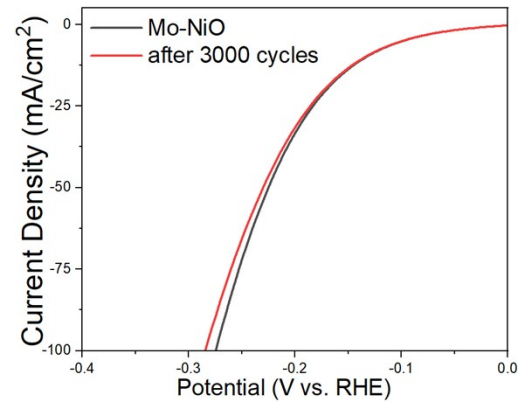


Figure S10. HER LSV curves for the Mo-NiO NPs before and after 3000 continuous CV scans.

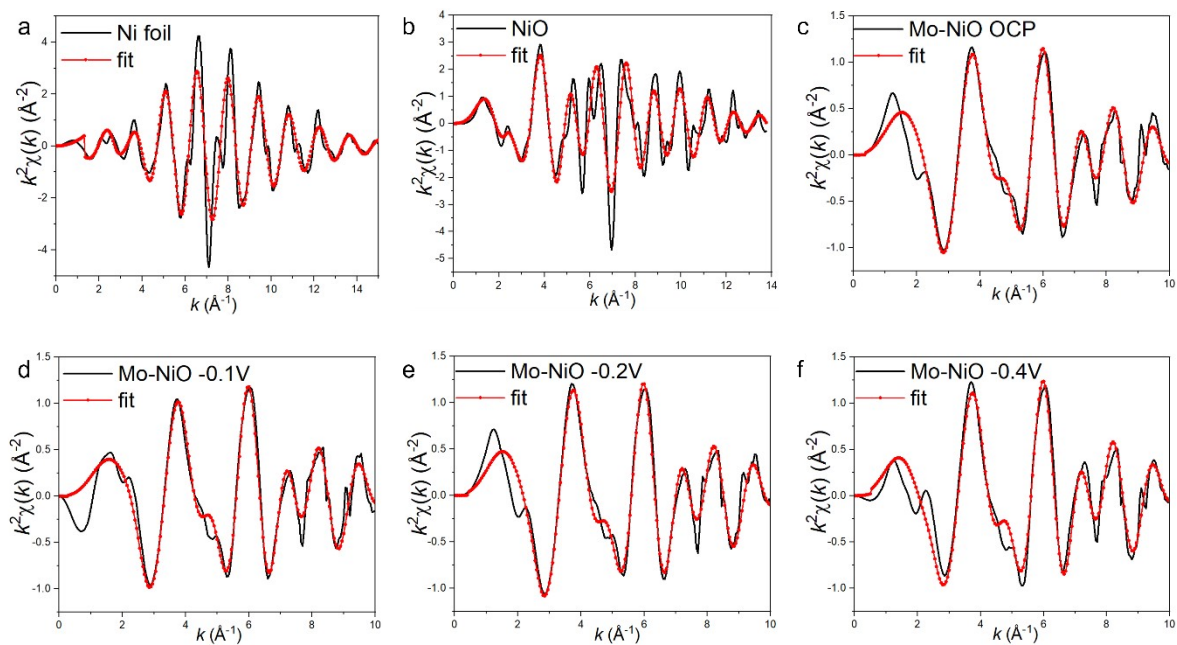


Figure S11. Ni K-edge EXAFS fitting (red dot line) for a) Ni foil, b) NiO and Mo-NiO at the potential of OCP, c) -0.1V, d) -0.2V and e) -0.4V vs. RHE shown in k -space. The data and the fits are shown in black and red dot line, respectively (k^2 -weighted). The curve-fit parameters in Table S2-3.

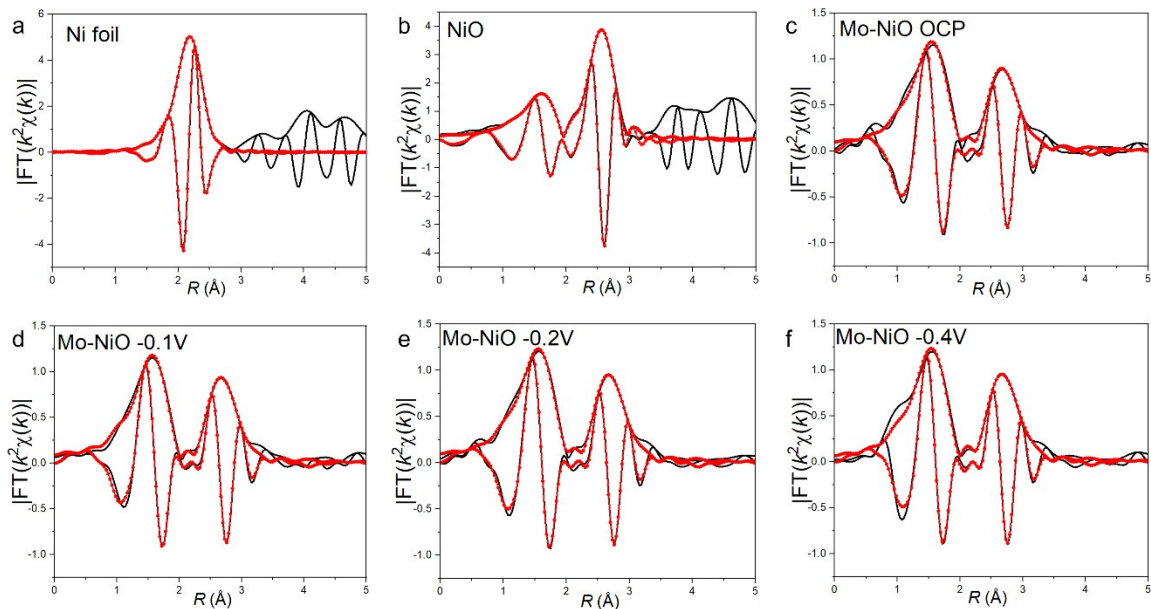


Figure S12. Ni K-edge EXAFS fitting (red dot line) for a) Ni foil, b) NiO and Mo-NiO at the potential of OCP, c) -0.1V, d) -0.2V and e) -0.4V vs. RHE shown in R -space, as the FT magnitude and imaginary components. The data and the fits are shown in black and red dot line, respectively (k^2 -weighted). The curve-fit parameters in Table S2-3.

Table S2. Curve-fit parameters for Ni K-edge EXAFS of Ni foil

Sample	Path	CN^a	<i>R</i>^a (Å)	$\Delta\sigma^2$^a (Å²)	ΔE_0^a (eV)	<i>S</i>₀²	R-factor
Ni foil	Ni-Ni	12	2.48(0.00)	0.0061(0.0002)	6.68(0.30)	0.784	0.001

^a CN, coordination number; *R*, distance between absorber and scatterer atoms; $\Delta\sigma^2$, disorder term; ΔE_0 , inner potential correction. Details of data analysis for Ni foil: *k* range: 3–15 Å⁻¹; *R* range: 1–3 Å. Error is reported inside the parentheses (accuracies). CN was fixed at the integer values shown.

Table S3. Curve-fit parameters for Ni K-edge EXAFS of NiO and Mo-NiO.

Sample	Path ^b	CN ^a	R^a (Å)	$\Delta\sigma^2$ ^a (Å ²)	ΔE_0^a (eV)	R-factor
NiO	Ni-O	7.08(0.66)	2.07(0.03)	0.0068(0.0026)	2.90(0.78)	0.009
	Ni-O-Ni	11.01(1.86)	2.98(0.03)	0.0075(0.0008)		
Mo-NiO OCP	Ni-O	5.28(0.60)	2.05(0.06)	0.008(0.002)	3.66(1.36)	0.015
	Ni-Ni	5.93(0.13)	3.11(0.05)	0.007(0.003)	0.55(2.00)	
Mo-NiO -0.1V	Ni-O	4.47(0.52)	2.05(0.06)	0.006(0.002)	2.74(1.41)	0.008
	Ni-Ni	5.61(0.22)	3.12(0.05)	0.005(0.003)	0.29(1.95)	
Mo-NiO -0.2V	Ni-O	5.47(0.53)	2.05(0.06)	0.007(0.001)	3.56(1.15)	0.010
	Ni-Ni	5.46(1.89)	3.12(0.04)	0.008(0.002)	0.71(1.65)	
Mo-NiO -0.4V	Ni-O	4.93(0.76)	2.04(0.07)	0.006(0.003)	5.14(1.85)	0.015
	Ni-Ni	5.68(3.01)	3.13(0.04)	0.006(0.004)	1.06(2.54)	

^a CN, coordination number; R , distance between absorber and scatterer atoms; $\Delta\sigma^2$, disorder term; ΔE_0 , inner potential correction. ^b S_0^2 was fixed at 0.784 by fitting the first single-scattering path of Ni foil. Details of data analysis for NiO: k range: 3–13 Å⁻¹; R range: 1–3.2 Å. Details of data analysis for Mo-NiO at different potential: k range: 2.5–10 Å⁻¹; R range: 1–3.5 Å. Error is reported inside the parentheses (accuracies).

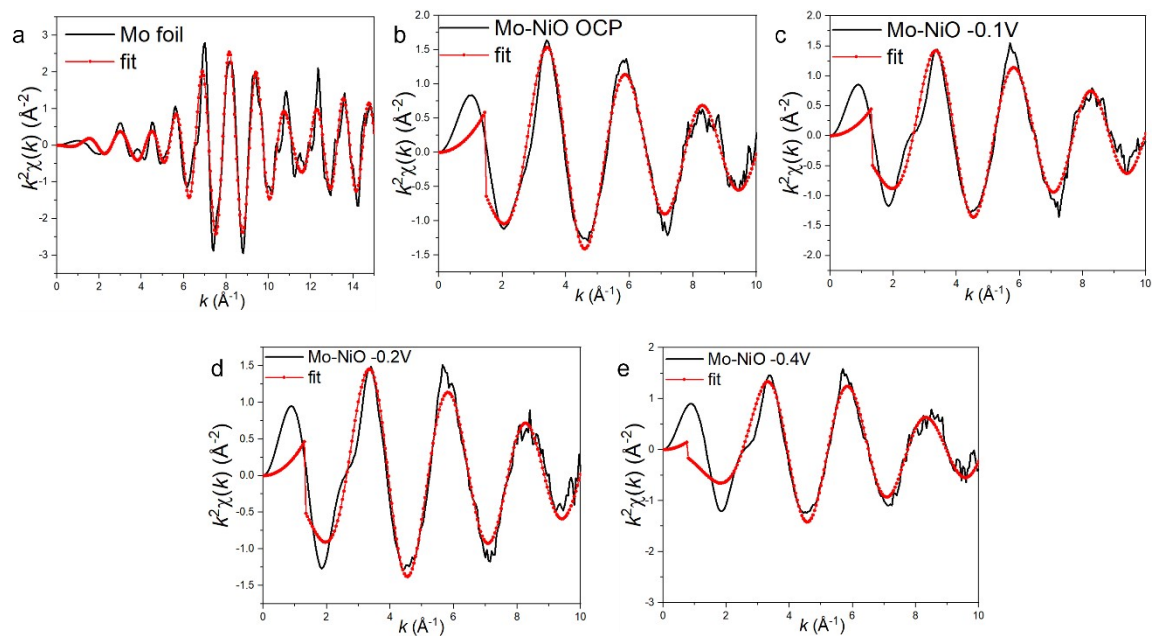


Figure S13. Mo K-edge EXAFS fitting (red dot line) for a) Mo foil, b) Mo-NiO at the potential of OCP, c) -0.1V, d) -0.2V and e) -0.4V vs. RHE shown in k -space. The data and the fits are shown in black and red dot line, respectively (k^2 -weighted). The curve-fit parameters in Table S4-5.

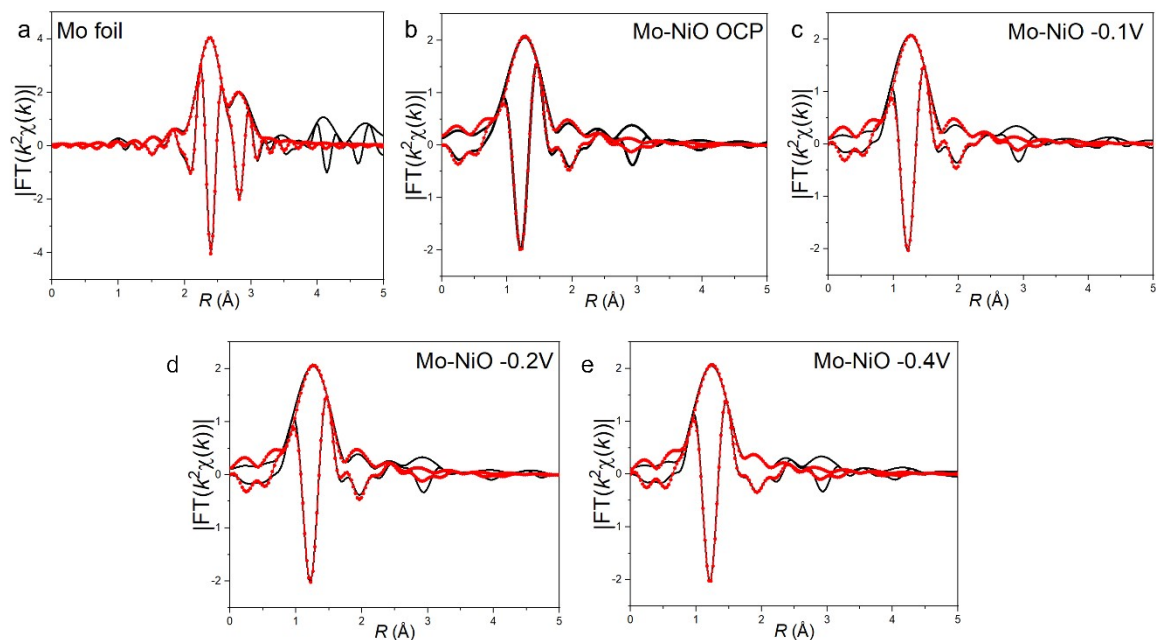


Figure S14. Mo K-edge EXAFS fitting (red dot line) for a) Mo foil, b) Mo-NiO at the potential of OCP, c) -0.1V, d) -0.2V and e) -0.4V vs. RHE shown in R -space, as the FT magnitude and imaginary components. The data and the fits are shown in black and red dot line, respectively (k^2 -weighted). The curve-fit parameters in Table S4-5.

Table S4. Curve-fit parameters for Mo K-edge EXAFS of Mo foil

Sample	Path	CN ^a	R^a (Å)	$\Delta\sigma^2$ ^a (Å ²)	ΔE_0^a (eV)	S_0^2	R-factor
Mo foil	Mo-Mo1	8	2.72(0.02)	0.0036(0.0015)			
					4.58(0.58)	0.885	0.005
	Mo-Mo2	6	3.17(0.03)	0.0036(0.0017)			

^a CN, coordination number; R , distance between absorber and scatterer atoms; $\Delta\sigma^2$, disorder term; ΔE_0 , inner potential correction. Details of data analysis for Ni foil: k range: 3–15 Å⁻¹; R range: 1–3.3 Å. Error is reported inside the parentheses (accuracies). CN was fixed at the integer values shown.

Table S5. Curve-fit parameters for Mo K-edge EXAFS of Mo-NiO.

Sample	Path ^b	CN ^a	<i>R</i> ^a (Å)	$\Delta\sigma^2$ ^a (Å ²)	ΔE_0 ^a (eV)	R-factor
Mo-NiO OCP	Mo-O	3.51(0.32)	1.75(0.02)	0.0018(0.0012)	8.37(1.32)	0.004
Mo-NiO -0.1V	Mo-O	3.27(0.36)	1.75(0.02)	0.0066(0.0013)	6.65(1.61)	0.007
Mo-NiO -0.2V	Mo-O	3.41(0.35)	1.75(0.02)	0.0012(0.0013)	6.57(1.52)	0.006
Mo-NiO -0.4V	Mo-O	3.43(0.71)	1.72(0.04)	0.0013(0.0025)	2.41(4.20)	0.004

^a CN, coordination number; *R*, distance between absorber and scatterer atoms; $\Delta\sigma^2$, disorder term; ΔE_0 , inner potential correction. ^b S_0^2 was fixed at 0.885 by fitting the first two single-scattering path of Mo foil. Details of data analysis for Mo-NiO at different potential: *k* range: 3–10 Å⁻¹; *R* range: 1–2.5 Å. Error is reported inside the parentheses (accuracies).

Reference

1. A. Joseph, A. Mathew and T. Thomas, *Int. J. Hydrogen Energy*, 2025, **99**, 15-25.
2. Z. Z. Liu, R. Y. Fan, N. Yu, Y. N. Zhou, X. Y. Zhang, B. Dong and Z. F. Yan, *Catalysts*, 2024, **14**.
3. G. Ghanashyam and H. Kyung Jeong, *FlatChem*, 2024, **43**, 100601.
4. S. Mishra, V. Sharma and V. Kulshrestha, *Langmuir*, 2025, **41**, 3516-3527.
5. G. Ghanashyam and H. K. Jeong, *Chem. Phys. Lett.*, 2023, **824**, 140546.
6. S. Marimuthu, A. Shankar and G. Maduraiveeran, *Chem. Commun.*, 2024, **60**, 1345-1348.
7. Z. Wang, J. Qu, Y. He, T. Xiong, Z. Huang, F. Wang and M. S. Balogun, *Mater. Chem. Front.*, 2023, **7**, 2683-2692.
8. S. Lai, K. Li, X. Lv, H. Ye, J. Wang, F. Dong and Z. Lin, *J. Power Sources*, 2025, **630**, 236089.
9. X. Ge, C. Zhang, M. Meng, Y. Song, S. Hu and Y. Gu, *ChemPlusChem*, 2024, **89**, e202300786.